



ELSEVIER

7 August 2000

PHYSICS LETTERS A

Physics Letters A 272 (2000) 389–394

www.elsevier.nl/locate/pla

3D nonlinear perturbative particle simulations of two-stream collective processes in intense particle beams

Hong Qin, Ronald C. Davidson^{*}, W. Wei-li Lee

Plasma Physics Laboratory, Princeton University, Princeton, NJ 08543, USA

Received 5 May 2000; accepted 15 June 2000

Communicated by M. Porkolab

Abstract

Collective processes in intense charged particle beams described self-consistently by the Vlasov–Maxwell equations are studied using a 3D multispecies nonlinear perturbative particle simulation method. The newly-developed Beam Equilibrium Stability and Transport (BEST) code has been used to simulate the nonlinear stability properties of intense beam propagation, surface eigenmodes in a high-intensity beam, and the electron–proton (e–p) two-stream instability observed in the Proton Storage Ring (PSR). © 2000 Elsevier Science B.V. All rights reserved.

For high-intensity accelerator applications ranging from spallation neutron sources to heavy ion fusion, space-charge effects on beam equilibrium, stability and transport properties become increasingly important. To understand these collective processes at high beam intensities, it is necessary to treat the beam dynamics self-consistently using the nonlinear Vlasov–Maxwell equations [1,2]. Recently, the δf formalism, a low-noise, nonlinear perturbative particle simulation technique, has been developed for intense beam applications, and applied to matched-beam propagation in a periodic focusing field [3,4] and other related studies. The present Letter reports recent advances in applying the δf formalism to investigate nonlinear collective processes in intense

charged particle beams. The BEST code [5] described here is a newly-developed 3D multispecies nonlinear perturbative particle simulation code, which can be applied to a wide range of important collective processes in intense beams, such as the electron two-stream interaction in proton storage rings [6–8] and electron storage rings [9–11], and periodically-focused beam propagation [12,13].

The theoretical model employed here is based on the nonlinear Vlasov–Maxwell equations. We consider a thin, continuous, high-intensity ion beam ($j = b$), with characteristic radius r_b propagating in the z -direction through background electron and ion components ($j = e, i$), each of which is described by a distribution function $f_j(\mathbf{x}, \mathbf{p}, t)$ [6,14,15]. The charge components propagate in the z -direction with characteristic axial momentum $\gamma_j m_j \beta_j c$, where $V_j = \beta_j c$ is the average directed axial velocity, and $\gamma_j = (1 - \beta_j^2)^{-1/2}$ is the relativistic mass factor of a j th species particle. While the nonlinear δf formalism outlined here is readily adapted to the case of a

^{*} Corresponding author. Tel: +1-609-243-3552; fax: +1-609-243-2749.

E-mail address: rdavidson@pppl.gov (R.C. Davidson).

periodic applied focusing field, for present purpose we make use of a *smooth-focusing* model in which the applied focusing force is described by

$$\mathbf{F}_j^{\text{foc}} = -\gamma_j m_j \omega_{\beta j}^2 \mathbf{x}_\perp, \quad (1)$$

where $\mathbf{x}_\perp = x\hat{e}_x + y\hat{e}_y$ is the transverse displacement from the beam axis, and $\omega_{\beta j} = \text{const.}$ is the effective applied betatron frequency for transverse oscillations. Furthermore, in a frame of reference moving with axial velocity $\beta_j c$, the motion of a j th species particle is assumed to be nonrelativistic. The space-charge intensity is allowed to be arbitrarily large, subject only to transverse confinement of the beam ions by the applied focusing force, and the background electrons are confined in the transverse plane by the space-charge potential $\phi(\mathbf{x}, t)$ produced by the excess ion charge. In the electrostatic and magnetostatic approximation, we represent the self-electric and self-magnetic fields as $\mathbf{E}^s = -\nabla\phi(\mathbf{x}, t)$ and $\mathbf{B}^s = \nabla \times A_z(\mathbf{x}, t)\hat{e}_z$. The nonlinear Vlasov–Maxwell equations in the six-dimensional phase space (\mathbf{x}, \mathbf{p}) can be approximated by [6,14]

$$\left\{ \frac{\partial}{\partial t} + \mathbf{v} \cdot \frac{\partial}{\partial \mathbf{x}} - \left[\gamma_j m_j \omega_{\beta j}^2 \mathbf{x}_\perp + e_j \left(\nabla\phi - \frac{v_z}{c} \nabla_\perp A_z \right) \right] \cdot \frac{\partial}{\partial \mathbf{p}} \right\} f_j(\mathbf{x}, \mathbf{p}, t) = 0, \quad (2)$$

and

$$\begin{aligned} \nabla^2 \phi &= -4\pi \sum_j e_j \int d^3 p f_j(\mathbf{x}, \mathbf{p}, t), \\ \nabla^2 A_z &= -\frac{4\pi}{c} \sum_j e_j \int d^3 p v_z f_j(\mathbf{x}, \mathbf{p}, t). \end{aligned} \quad (3)$$

In the nonlinear δf formalism [16,17], we divide the total distribution function into two parts, $f_j = f_{j0} + \delta f_j$, where f_{j0} is a *known* solution to the nonlinear Vlasov–Maxwell Eqs. (2) and (3), and the numerical simulation is carried out to determine only the detailed nonlinear evolution of the perturbed distribution function δf_j . This is accomplished by advancing the weight function defined by $w_j \equiv \delta f_j / f_j$, together with the particles' positions and momenta. The equations of motion for the particles,

obtained from the characteristics of the nonlinear Vlasov Eq. (2), are given by

$$\begin{aligned} \frac{d\mathbf{x}_{ji}}{dt} &= (\gamma_j m_j)^{-1} \mathbf{p}_{ji}, \\ \frac{d\mathbf{p}_{ji}}{dt} &= -\gamma_j m_j \omega_{\beta j}^2 \mathbf{x}_{\perp ji} - e_j \left(\nabla\phi - \frac{v_{zji}}{c} \nabla_\perp A_z \right). \end{aligned} \quad (4)$$

Here the subscript ‘ ji ’ labels the i th simulation particle of the j th species. The weight functions w_j , as functions of phase space variables, are carried by the simulation particles, and the dynamical equations for w_j are easily derived from the definition of w_j and the nonlinear Vlasov Eq. (2). Following some algebra, we obtain [3–5,16,17]

$$\begin{aligned} \frac{dw_{ji}}{dt} &= -(1 - w_{ji}) \frac{1}{f_{j0}} \frac{\partial f_{j0}}{\partial \mathbf{p}} \cdot \delta \left(\frac{d\mathbf{p}_{ji}}{dt} \right), \\ \delta \left(\frac{d\mathbf{p}_{ji}}{dt} \right) &\equiv -e_j \left(\nabla\delta\phi - \frac{v_{zji}}{c} \nabla_\perp \delta A_z \right), \end{aligned} \quad (5)$$

where $\delta\phi = \phi - \phi_0$ and $\delta A_z = A_z - A_{z0}$. Here, the equilibrium solutions (ϕ_0, A_{z0}, f_{j0}) solve the steady-state ($\partial/\partial t = 0$) Vlasov–Maxwell Eqs. (2) and (3) with $\partial/\partial z = 0$ and $\partial/\partial \theta = 0$. A wide variety of axisymmetric equilibrium solutions to Eqs. (2) and (3) have been investigated in the literature. The perturbed distribution δf_j is obtained through the weighted Klimontovich representation [1]

$$\delta f_j = \frac{N_j}{N_{sj}} \sum_{i=1}^{N_{sj}} w_{ji} \delta(\mathbf{x} - \mathbf{x}_{ji}) \delta(\mathbf{p} - \mathbf{p}_{ji}), \quad (6)$$

where N_j is the total number of actual j th species particles, and N_{sj} is the total number of *simulation* particles for the j th species. Maxwell's equations are also expressed in terms of the perturbed fields and perturbed density according to

$$\begin{aligned} \nabla^2 \delta\phi &= -4\pi \sum_j e_j \delta n_j, \\ \nabla^2 \delta A_z &= -\frac{4\pi}{c} \sum_j \delta j_{zj}, \end{aligned} \quad (7)$$

where

$$\begin{aligned} \delta n_j &= \int d^3p \delta f_j(\mathbf{x}, \mathbf{p}, t) \\ &= \frac{N_j}{N_{sj}} \sum_{i=1}^{N_{sj}} w_{ji} S(\mathbf{x} - \mathbf{x}_{ji}), \\ \delta j_{zj} &= e_j \int d^3p v_{zj} \delta f_j(\mathbf{x}, \mathbf{p}, t) \\ &= \frac{e_j N_j}{N_{sj}} \sum_{i=1}^{N_{sj}} v_{zji} w_{ji} S(\mathbf{x} - \mathbf{x}_{ji}). \end{aligned} \quad (8)$$

Here, $S(\mathbf{x} - \mathbf{x}_{ji})$ is a shape function distributing particles on the grids in configuration space.

The nonlinear particle simulations are carried out by iteratively advancing the particle motions, including the weights they carry, according to Eqs. (4) and (5), and updating the fields by solving the perturbed Maxwell's Eqs. (7) with appropriate boundary conditions at the cylindrical, perfectly conducting wall. Even though it is a perturbative approach, the δf method is *fully nonlinear* and simulates completely the original nonlinear Vlasov–Maxwell equations. Compared with conventional particle-in-cell simulations, the noise level in δf simulations is significantly reduced. The δf method can also be used to study *linear* stability properties, provided the factor $(1 - w_{ji})$ in Eq. (5) is approximated by unity, and the forcing term in Eq. (4) is replaced by the unperturbed force.

Implementation of the 3D multispecies nonlinear δf simulation method described above is embodied in the BEST code [16,17]. The code advances the particle motions using a leap-frog method, and solves Maxwell's equations in cylindrical geometry. For those fast particle motions which require much larger sampling frequency than the frequency of the mode being studied, the code uses an adiabatic field pusher to advance the particles many time steps without solving for the perturbed fields.

We first present application of the code to a single-species thermal equilibrium ion beam ($j = b$) in a constant focusing field. It is assumed that the beam is centered inside a cylindrical pipe with perfectly conducting wall located at $r = r_w$, and that equilibrium properties depend only on the radial

coordinate $r = (x^2 + y^2)^{1/2}$. The isotropic thermal equilibrium distribution function in the phase space (r, \mathbf{p}) is given by [1,14]

$$\begin{aligned} f_{b0}(r, \mathbf{p}) &= \frac{\hat{n}_b}{(2\pi\gamma_b m_b T_b)^{3/2}} \\ &\times \exp\left\{-\frac{p_\perp^2/2\gamma_b m_b + \gamma_b m_b \omega_{pb}^2 r^2/2 + e_b(\phi_0 - \beta_b A_{z0})}{T_b}\right\} \\ &\times \exp\left\{-\frac{(p_z - \gamma_b m_b \beta_b c)^2}{2\gamma_b m_b T_b}\right\}, \end{aligned} \quad (9)$$

where \hat{n}_b is the number density of beam particles at $r = 0$, and $T_b = \text{const.}$ is the temperature of the beam ions in energy units. The equilibrium self-field potentials ϕ_0 and A_{z0} can be determined numerically from the nonlinear Maxwell's equations in Eq. (3). As an example, we examine the nonlinear propagation properties of a heavy ion beam with $\gamma_b = 1.08$, mass number $A = 133$, and normalized space-charge intensity $\hat{\omega}_{pb}^2/2\gamma_b^2\omega_{pb}^2 = 0.95$. Here, $\hat{\omega}_{pb}^2 = 4\pi\hat{n}_b^2 e_b^2/\gamma_b m_b$ is the relativistic plasma frequency-squared on axis ($r = 0$). A random initial perturbation is introduced into the system, and the beam is propagated from $t = 0$ to $t = 1200\tau_\beta$, where $\tau_\beta \equiv \omega_{pb}^{-1}$. The simulation results show that the perturbations do not grow and the beam propagates quiescently over large distance, which agrees with the nonlinear stability theorem [18] for the choice of monotonically-decreasing equilibrium distribution function in Eq. (9).

As a second example, we study the linear surface mode for perturbations about a thermal equilibrium ion beam in the space-charge-dominated regime, with flat-top density profile. These modes are of practical interest because they can be destabilized by a two-stream electron-ion interaction when background electrons are present [6–8]. The BEST code, operating in its linear stability mode, has recovered very well-defined eigenmodes with mode structures and eigenfrequencies which agree well with theoretical predications [6]. For the dipole mode with azimuthal mode number $l = 1$, the dispersion relation is given by [6]

$$\omega = k_z V_b \pm \frac{\hat{\omega}_{pb}}{\sqrt{2}\gamma_b} \sqrt{1 - \frac{r_b^2}{r_w^2}}, \quad (10)$$

where r_b is the radius of the beam edge, and r_w is location of the conducting wall. In Eq. (10), $\hat{\omega}_{pb}^2 = 4\pi\hat{n}_b e_b^2 / \gamma_b m_b$ is the ion plasma frequency-squared, and $\hat{\omega}_{pb} / \sqrt{2} \gamma_b = \omega_{\beta b}$ has been assumed in the space-charge-dominated limit. The dependence of the eigenfrequency on r_w/r_b obtained from the simulations agree very well with the theoretical predictions of Eq. (10) [17].

In a high-intensity ion beam, the surface mode described above can be destabilized by the presence of a background electron population [6–8]. This instability is basically of the two-stream type, and is strongest when the ions are relatively cold in the propagation direction. The directed velocity difference, $V_b - V_e$, between the beam ions and the background electrons provides the free energy for the collective modes to grow. The instability observed in the Proton Storage Ring [7,8] is believed to have this two-stream characteristic.

We present here simulation results for the electron–proton two-stream instability with moderate space-charge intensity corresponding to $\hat{\omega}_{pb}^2 / 2\gamma_b^2 \omega_{\beta b}^2 = 0.074$, $\gamma_b = 1.85$, and $m_e/m_b = 1/1836$. The equilibrium distribution functions f_{j0} are chosen to be thermal equilibrium distributions for both species with $T_{b\perp} / \gamma_b m_b V_b^2 = 3.61 \times 10^{-6}$, $T_{e\perp} / \gamma_b m_b V_b^2 = 5.86 \times 10^{-7}$, and $f \equiv \hat{n}_e / \hat{n}_b = 0.1$, $V_e = 0$, and $\omega_{\beta e} = 0$ (stationary electrons). These

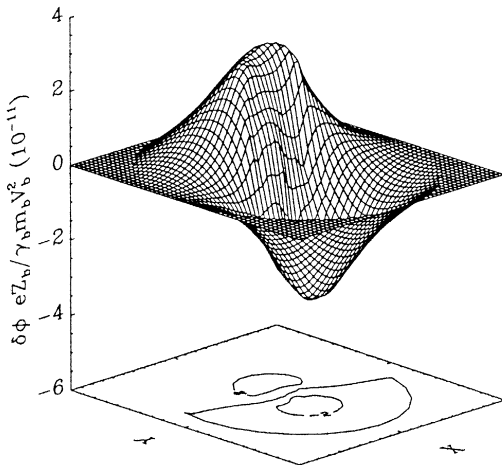


Fig. 1. The x - y projection (at fixed value of z) of the perturbed electrostatic potential $\delta\phi(x, y, t)$ at $\omega_{\beta b} t = 200$ for the perturbations growing from a small initial level.

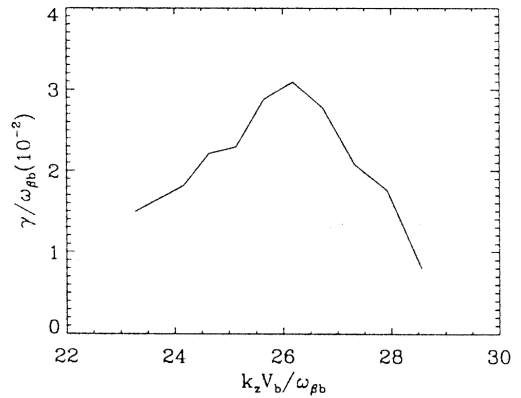


Fig. 2. Plots of the linear growth rate $\gamma = \text{Im } \omega$ versus $k_z V_b / \omega_{\beta b}$.

system parameters correspond to the typical operating parameters in the PSR experiment [7,8]. In the simulations of the e–p instability, we take the background distribution functions $f_{j0}(r, \mathbf{p})$ to be the *bi-Maxwellian* generalization of Eq. (9), with temperature $T_{j\perp} = \text{const.}$ in the x - y plane, and temperature $T_{j\parallel} = \text{const.}$ in the z -direction. Because the e–p instability is strongest when the beam ions are *cold* in the parallel direction [6] (no Landau damping by parallel kinetic effects), we take $T_{b\parallel} = 0$ and $T_{e\parallel} = 0$ in the simulations presented in Figs. 1, 2 and 3. The stabilizing influence of longitudinal Landau damping by parallel ion kinetic effects at increasing values of $T_{b\parallel} / T_{b\perp}$ is illustrated in Fig. 4. Shown in Fig. 1 is a typical unstable case, where the x - y projection (at fixed value of z) of the perturbed space-charge potential $\delta\phi(x, y, t)$ grows exponentially with time during the linear phase of the instability. Clearly, the

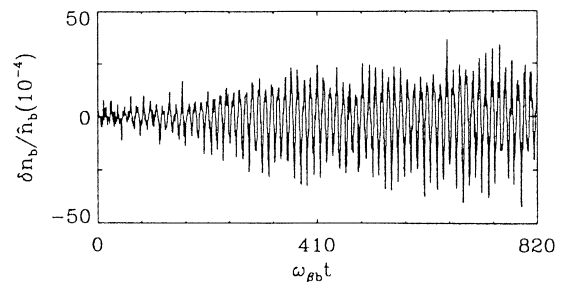


Fig. 3. Linear and nonlinear phases of the electron–proton instability.

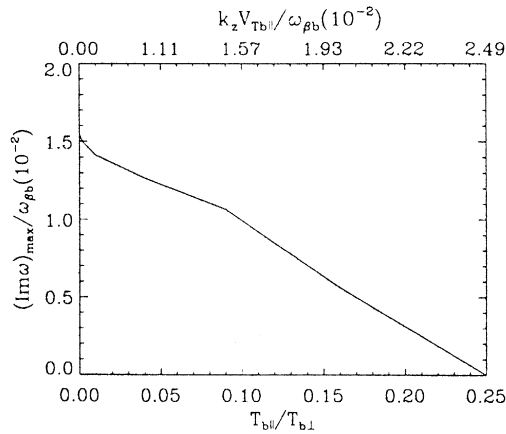


Fig. 4. The maximum linear growth rate $(\text{Im } \omega)_{\text{max}}$ of the electron–proton instability decreases as the longitudinal temperature of the beam ions increases.

unstable mode is a dipole mode with azimuthal mode number $l = 1$ [17].

A plot of the instability growth rate $\gamma = \text{Im } \omega$ versus $k_z V_b / \omega_{\beta b}$, with other parameters kept constant, is shown in Fig. 2. The $k_z V_b / \omega_{\beta b}$ dependence of the growth rate is qualitatively consistent with the analytical results obtained for uniform-density beams [6]. The important physics here is that only for a certain range of $k_z V_b / \omega_{\beta b}$ can the collective mode of the beam ions effectively resonate with the electrons and produce instability. Simulation results show that the value of $T_{e\perp} / T_{b\perp}$ has an important effect on the growth rate. In order to maximize their energy exchange with the beam ions, the electrons must spatially overlap the region where the eigenmode of the beam ions is localized (approximately the region with the largest transverse gradient in ion density), which requires sufficiently large $T_{e\perp} / T_{b\perp}$. The electrons are radially confined by the space-charge potential of the beam ions, and the perpendicular electron temperature determines the radial extent of the electron density profile. The growth rate is therefore strongly dependent on $T_{e\perp} / T_{b\perp}$ [17]. For the system parameters listed above, the growth rate $\gamma = 0.031 \omega_{\beta b}$ when $T_{e\perp} / T_{b\perp} = 0.130$, but becomes undetectable over $360 \omega_{\beta b}^{-1}$ when $T_{e\perp} / T_{b\perp} = 0.018$.

Finally, for $T_{e\perp} / T_{b\perp} = 0.130$, the simulation results for the linear and nonlinear phases of the instability are shown in Fig. 3, where the density

perturbation amplitude δn_b at one spatial location is plotted versus $\omega_{\beta b} t$. We see clearly the initial linear growth phase and the nonlinear saturation of the instability. For the parameters considered here, the instability nonlinearly saturates at $t \sim 400 \omega_{\beta b}^{-1}$ at a normalized amplitude of $\delta n_b / \hat{n}_b \sim 0.3\%$.

In the simulation results for the e–p instability presented above, we have assumed cold beam ions in the longitudinal direction ($T_{b||} = 0$) to maximize the growth rate of the instability. In general, when the longitudinal temperature of the beam ions is finite, Landau damping by parallel ion kinetic effects provides a mechanism that reduces the growth rate [17]. The decrease in the linear growth rate due to Landau damping of the unstable modes can be estimated to be of order $k_z v_{Tb||}$, where $v_{Tb||} = (2T_{b||} / \gamma_b m_b)^{1/2}$. Shown in Fig. 4 is a plot of the maximum linear growth rate $(\text{Im } \omega)_{\text{max}}$ versus $T_{b||} / T_{b\perp}$ and $k_z v_{Tb||}$ obtained in numerical simulations of the e–p instability using the BEST code. As evident from the figure, the growth rate decreases dramatically as $T_{b||} / T_{b\perp}$ and $k_z v_{Tb||}$ increase. When $T_{b||}$ is high enough that $k_z v_{Tb||}$ is comparable to the linear growth rate for the $T_{b||} = 0$ case, the mode is stabilized by longitudinal Landau damping by the beam ions. Because the phase velocity of the mode in the longitudinal direction is far removed from the electron velocity distribution, $|\omega / k_z| \gg V_e + v_{Te||}$, we do not expect the longitudinal electron temperature to affect significantly the growth rate of the instability.

In conclusion, a 3D multispecies nonlinear perturbative particle simulation method has been developed to study collective processes in intense charged particle beams described self-consistently by the Vlasov–Maxwell equations. The simulation results show that an isotropic thermal equilibrium ion beam in a constant focusing field is nonlinearly stable and can propagate quiescently over hundreds of lattice periods [18]. Introducing a background component of electrons, a strong electron–proton (e–p) two-stream instability is observed in the simulations when $T_{b||}$ is sufficiently small. Several properties of this instability have been investigated numerically, and are found to be in qualitative agreement with theoretical predictions. Most importantly, the simulations show that the two-stream instability can be stabilized by a modest spread in axial momentum of the beam parti-

cles. Further details will be presented in a related publication [17].

Acknowledgements

This research was supported by the Department of Energy and the Short Pulse Spallation Source project and LANSCE Division of Los Alamos National Laboratory.

References

- [1] R.C. Davidson, *Physics of Nonneutral Plasmas*, Addison-Wesley Co. Publishing, Reading, MA, 1990, and references therein.
- [2] A.W. Chao, *Physics of Collective Beam Instabilities in High Energy Accelerators*, Wiley, New York, 1993.
- [3] W.W. Lee, Q. Qian, R.C. Davidson, *Phys. Lett. A* 230 (1997) 347.
- [4] P.H. Stoltz, R.C. Davidson, W.W. Lee, *Phys. Plasmas* 6 (1999) 298.
- [5] H. Qin, R.C. Davidson, W.W. Lee, *Proc. 1999 Part. Accel. Conf.* 3 (1999) 1626.
- [6] R.C. Davidson, H. Qin, P.H. Stoltz, T.-S. Wang, *Phys. Rev. Special Topics Accel. and Beams* 2 (1999) 54401, and references therein.
- [7] D. Neuffer, E. Colton, D. Fitzgerald, T. Hardek, R. Hutson, R. Macek, M. Plum, H. Thiessen, T.-S. Wang, *Nucl. Instr. Methods Phys. Res. A* 321 (1992) 1.
- [8] R. Macek, *Proc. Workshop on Space Charge Physics in High Intensity Hadron Rings*, Am. Inst. Conf. Proc. 448 (1998) 116.
- [9] M. Izawa, Y. Sato, T. Toyomasu, *Phys. Rev. Lett.* 74 (1995) 5044.
- [10] J. Byrd, A. Chao, S. Heifets, M. Minty, T.O. Roubenheimer, J. Seeman, G. Stupakov, J. Thomson, F. Zimmerman, *Phys. Rev. Lett.* 79 (1997) 79.
- [11] K. Ohmi, *Phys. Rev. E* 55 (1997) 7550.
- [12] R.C. Davidson, H. Qin, P.J. Channell, *Phys. Rev. Special Topics Accel. and Beams* 2 (1999) 074401.
- [13] P.J. Channell, *Phys. Plasmas* 6 (1999) 982.
- [14] R.C. Davidson, C. Chen, *Part. Accel.* 59 (1998) 175.
- [15] I. Hofmann, L. Laslett, L. Smith, I. Haber, *Part. Accel.* 13 (1983) 145.
- [16] H. Qin, R.C. Davidson, W.W. Lee, *Proc. Workshop on Instabilities of High Intensity Hadron Beams in Rings*, American Institute Conference Proc. 496 (1999) 295.
- [17] H. Qin, R.C. Davidson, W.W. Lee, submitted for publication, 2000.
- [18] R.C. Davidson, *Phys. Rev. Lett.* 81 (1998) 991.